

---

# CLOSENESS AND UNCERTAINTY AWARE ADVERSARIAL EXAMPLES DETECTION IN ADVERSARIAL MACHINE LEARNING

---

**Omer Faruk Tuna**  
Işık University  
Istanbul, Turkey  
omer.tuna@isikun.edu.tr

**Ferhat Ozgur Catak**  
Simula Research Lab.  
Fornebu, Norway  
ozgur@simula.no

**M. Taner Eskill**  
Işık University  
Istanbul, Turkey  
taner.eskil@isikun.edu.tr

## ABSTRACT

Deep neural network (DNN) architectures are considered to be robust to random perturbations. Nevertheless, it was shown that they could be severely vulnerable to slight but carefully crafted perturbations of the input, which are termed as adversarial samples. In recent years, numerous studies have been conducted to increase the reliability of DNN models by distinguishing adversarial samples from regular inputs. In this work, we explore and assess the usage of 2 different groups of metrics in detecting adversarial samples: the ones which are based on the uncertainty estimation using Monte-Carlo Dropout Sampling and the ones which are based on closeness measures in the subspace of deep features extracted by the model. We also introduce a new feature for adversarial detection, and we show that the performances of all these metrics heavily depend on the strength of the attack being used.

## 1 Introduction

Machine learning (ML) applications are transforming our everyday lives and the artificial intelligence technology is becoming an integral part of our civilization. As the artificial intelligence technology advances, it becomes a key component of many sophisticated tasks that have direct effect on humans. In the last few years, deep neural networks (DNNs) achieved state-of-the-art performances on different number of supervised learning tasks, which led them to become widely used in many fields such as medical diagnosis, computer vision, machine translation, speech recognition and autonomous vehicles [1, 2, 3, 4]. However, there exist serious concerns on how to make deep neural networks an integral part of our lives while ensuring utmost security and reliability.

Although DNNs have proven their usefulness in the real-world applications for many complex problems, they have thus far failed to overcome the challenges faced by deliberately manipulated data, which are known as adversarial inputs [5]. Therefore, a recent problem facing the ML community is to furnish the state of the art algorithms with tools that actively detect and avert adversarial attacks, making them robust to such inputs [6]. These adversarial attacks are based on perturbing the input instance in a direction which maximizes the possibility of incorrect decision making, thus results in a false prediction. They can lead to a loss of the model's prediction performance as the algorithm is unable to distinguish an adversarial input from a legitimate one. Moreover, attacks utilizing the vulnerability of DNNs can seriously hamper the security of these ML based systems, sometimes with devastating consequences. In the case of medical applications, the perturbation attack can lead to an incorrect diagnosis of disease and thus can cause severe harm to a patient's health and also damage healthcare economy [7]. In another domain, many state-of-the-art autonomous navigation algorithms use DNNs to drive vehicles in traffic without human intervention while avoiding accidents. A wrong decision by an autonomous navigation algorithm due to an adversarial attack could cause a fatal accident [8, 9]. Thus, defending against adversarial attempts and increasing the robustness of the deep architectures without compromising performance is of crucial importance.

Since the first discovery of adversarial examples by Szegedy et al. [10] in 2013, researchers developed several methods to understand and defend against the craftily manipulated instances. In the domain of cyber security, the first step of defence is considered to be the awareness of a malicious attempt. Thus, the primary goal in this field has been to distinguish adversarial samples from regular or legitimate inputs, and evading such attempts based on this awareness.

In this study, we aim to analyze different metrics in adversarial sample detection. Our first step is to analyze uncertainty metrics obtained from MC Dropout sampling to quantify its prediction accuracy. We used softmax decision making together with variance, entropy, mutual information and model confidence to quantify the model’s uncertainty. We showed that the quantified uncertainty in prediction time is strongly correlated with the strength of adversarial attempt, but only within a *low confidence window* in which the impact of applied perturbation starts to change the classifier’s prediction. We observed that within this window, the choice of combined usage of uncertainty metrics yields better performance. Moreover, we showed that for the *high confidence window*, where applied perturbation has no resulting impact on the uncertainty metrics and predicted class, another group of metric based on the closeness of low dimensional representation of training and test samples does a better job in detecting adversarial examples. We also introduced a novel approach to quantify the closeness using Kullback-Leibler Divergence (KL Divergence) loss using the activations of the last hidden layer. An empirical validation was systematically conducted in the prediction time for some of the well-known adversarial machine learning attacks.

To sum up; our main contributions for this paper are:

- We introduce a new metric to quantify the closeness of an input sample’s representation with its predicted class data manifold in the subspace of last hidden layer activations. It is a simpler and computationally efficient alternative to density estimation approach.
- We show that there is no single metrics which works well in every condition, and an ensemble approach of using different metrics should be considered.

The rest of the paper is organized as follows: Section 2 briefly introduces the related work. Section 3 describes preliminary information about the adversarial attack types, model uncertainty quantification and closeness metrics. Section 4 shows the system model. Section 5 shows our experimental setup and results. Section 6 concludes this paper.

## 2 Related Work

Since the discovery of DNN’s vulnerability to adversarial attacks [10], a vast amount of research has been conducted in both devising new adversarial attacks and defending against these attacks with more robust DNN models [11]. Defence against adversarial attacks can be divided into two categories; (i) improving the robustness of classifiers to existing attack types, (ii) methods for detecting adversarial samples. In our research, we focus on the detection of the adversarial samples.

Goodfellow et al. [12] demonstrated that crafting adversarial examples and including them in model training increases the robustness of these models to related adversarial attacks. The degree of robustness attained by such adversarial training depends on the strength of the adversarial examples used in the training stage. Papernot et al. [13] proposed the defensive distillation technique which involves training a DNN (known as the student) with the softmax outputs of another neural network (known as the teacher) that was trained on the training data and can be seen as a way of preventing the network from fitting too tightly to the data. However, Carlini & Wagner [14] soon showed that defensive distillation method could indeed simply be broken with a stronger attack.

Feinman et al. [15] focused on detecting adversarial samples through two measures; estimations of uncertainty and the kernel density. They formulated the uncertainty estimate as the variance of a Bayesian distribution which is obtained from the neural network model with dropout. They estimated the kernel density through the activations of the last hidden layer. However, it is also possible to model uncertainty from a dropout network through entropy, mutual information and model confidence. Ma et al. [16] proposed to detect adversarial samples using an auxiliary classifier that is trained to use an expansion-based measure; local intrinsic dimensionality. Metzen et al. [17] proposed augmenting a DNN with an additional *detector* subnetwork, trained on the binary classification task of normal and adversarial samples.

Apart from adversarial sample detection, uncertainty metric obtained by MC dropout sampling were also used to relate errors in the prediction from the classifier. In the medical imaging domain, Combalia et al. [18] used variance, entropy and Bhattacharyya Coefficient metrics in the problem of skin lesion classification and assessed the performance of each individual metric. However, they did not use a combination of these metrics to increase performance rates. Leibig et al. [19] used dropout based Bayesian uncertainty measures for DNN in diagnosing diabetic retinopathy and increased the diagnostic performance. They do so by referring a subset of difficult cases for further inspection based on a computed measure of uncertainty.

Although numerous methods have been proposed so far to detect adversarial samples and abnormalities in model prediction, there is not enough study in literature so far to evaluate the performances of these methods and a guideline to show the effectiveness of them under varying degree of threat levels. In this study, we aimed to fill this gap.

### 3 Preliminaries

In this section, we will introduce adversarial machine learning and its related concepts, model uncertainty, uncertainty metrics and closeness metrics.

#### 3.1 Adversarial Machine Learning

Adversarial machine learning is a technique that attempts to fool deep learning models by using deliberately crafted deceptive input. In this work, we assume that the attackers apply a probabilistic and white box approach to select the best parameters to manipulate the input data and feed into the model. Deep learning algorithms contain many vulnerabilities and weaknesses which make them difficult to defend in the context of adversarial machine learning. For instance, they are often sensitive to small changes in the input data, which can result in unexpected results in the final output of the model. Figure 1 shows how an adversary would exploit such a vulnerability and manipulate the model through the use of carefully crafted perturbation applied to the input data.

Adversarial machine learning is a technique for evading or fooling the deep learning models by using an adversary to extract or manipulate information in the training data [20]. The attackers apply a probabilistic and white box approach to a model by selecting the best parameters to manipulate the input data and feed into the model. The deep learning algorithms contain many vulnerabilities and weaknesses which make them difficult to defend against in the context of adversarial machine learning. For instance, they are often sensitive to small changes in the input data, which can result in unexpected results in the final output of the model. Figure 1 shows how an adversary would exploit such a vulnerability and manipulate the model through the use of carefully crafted perturbation applied to the input data.

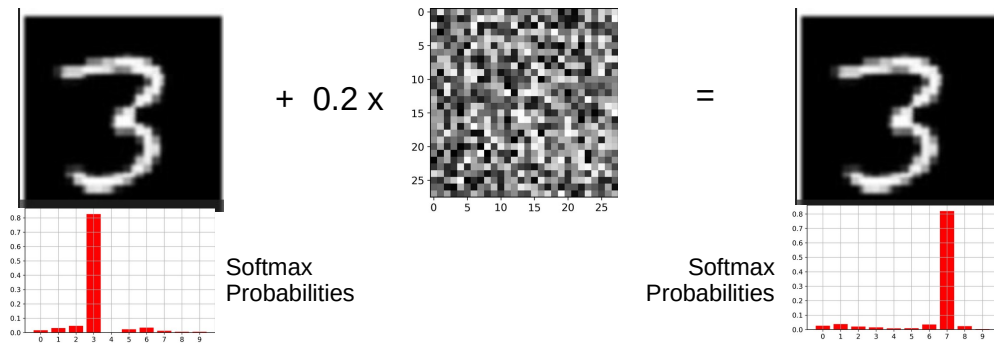


Figure 1: The figure shows an adversarial example in character recognizing. The malicious input is expressed using the original image and the precisely perturbations such that a digit-3 is misclassified as a digit-7 with high confidence.

The adversarial machine learning is an umbrella term used to describe a variety of forms of malicious input generation. There are several practical techniques which can be used to generate adversarial data based on a particular pattern and to produce a unique result. These include learning the shape of the input data and understanding the nature of the target data. In this study, we generated the adversarial instances using fast-gradient sign method, iterative-gradient sign method and projected gradient descent. As a result of our approach, we created a set of training-style adversarial instances to test the accuracy of the adversarial techniques.

##### 3.1.1 Fast-Gradient Sign Method

Fast-Gradient Sign Method (FGSM) is one of the first and most popular adversarial attacks to date. It is described by Goodfellow et al. [12]. FGSM uses the gradient of the loss function to determine in which direction the pixel's intensity of the source image should be changed to minimize the loss function of the model; then, it shifts all pixels simultaneously in the opposite direction to maximize the loss. For a model with classification loss function described as  $L(\theta, \mathbf{x}, y)$  where  $\theta$  represents the parameters of the model,  $\mathbf{x}$  is the model input (sample input image in our case),  $y_{true}$  is the label of our input, we can generate adversarial samples using below formula:

$$\mathbf{x}^* = \mathbf{x} + \epsilon \text{sign}(\nabla_{\mathbf{x}} L(\theta, \mathbf{x}, y_{true})) \quad (1)$$

One last key point about FGSM is that it is not designed to be optimal but fast. That means it is not designed to produce the minimum required adversarial perturbation. Besides, the success ratio of this method is relatively in low  $\epsilon$  values compared to other attack types.

### 3.1.2 Iterative Gradient Sign Method

Kurakin et al. [21] introduce a simple improvement to the FGSM where instead of taking a single step of size  $\epsilon$  in the direction of the gradient sign, multiple smaller steps  $\alpha$  are taken, and the same *epsilon* clips the result. This attack type is often referred to as Basic Iterative Method (BIM), and it is just FGSM applied to an input image iteratively. Generating perturbed images is given by

$$\begin{aligned} \mathbf{x}^* &= \mathbf{x} \\ \mathbf{x}_{N+1}^* &= \text{Clip}_{x,\epsilon}\{\alpha \text{sign}(\nabla_{\mathbf{x}}L(\mathbf{x}_N^*, y_{true}))\} \end{aligned} \quad (2)$$

where  $\mathbf{x}$  is the input image,  $\mathbf{x}^*$  is the produced adversarial image at  $i$ th iteration,  $L$  is the loss function of the model,  $y_{true}$  is true label for input image,  $\epsilon$  is a tunable parameter, limiting maximum level of perturbation in given  $l_{norm}$ ,  $\alpha$  is the step size.

BIM attack is more successful than the FGSM in terms of attack success ratio [22]. By adjusting the  $\epsilon$  parameter, the attacker can manipulate how far past the decision boundary an adversarial sample will be pushed.

### 3.1.3 Projected Gradient Descent

Projected Gradient Descent (PGD), introduced by Madry et al. [23], perturbs a normal example  $\mathbf{x}$  for a number of  $i$  steps with a small step size. Different from BIM, after each step of perturbation, PGD projects the adversarial example back onto the  $\epsilon$ -ball of input sample, instead of clipping. Moreover, PGD uses random start, which can be described as:

$$\mathbf{x}_0 = \mathbf{x} + U^d(-\epsilon, +\epsilon) \quad (3)$$

where  $U^d(-\epsilon, +\epsilon)$  is the uniform distribution between  $-\epsilon, +\epsilon$  and of the same  $d$  dimensions as  $\mathbf{x}$ .

## 3.2 Preliminary Attack Results

Figure 2 shows the success ratios of the three attacks used in this study for different epsilon ( $\epsilon$ ) values on the MNIST (Digit) and MNIST (Fashion) datasets. For all the attacks, we have used  $l_{inf}$  norm as the distance metric, which shows the maximum allowable perturbation amount for each pixel.

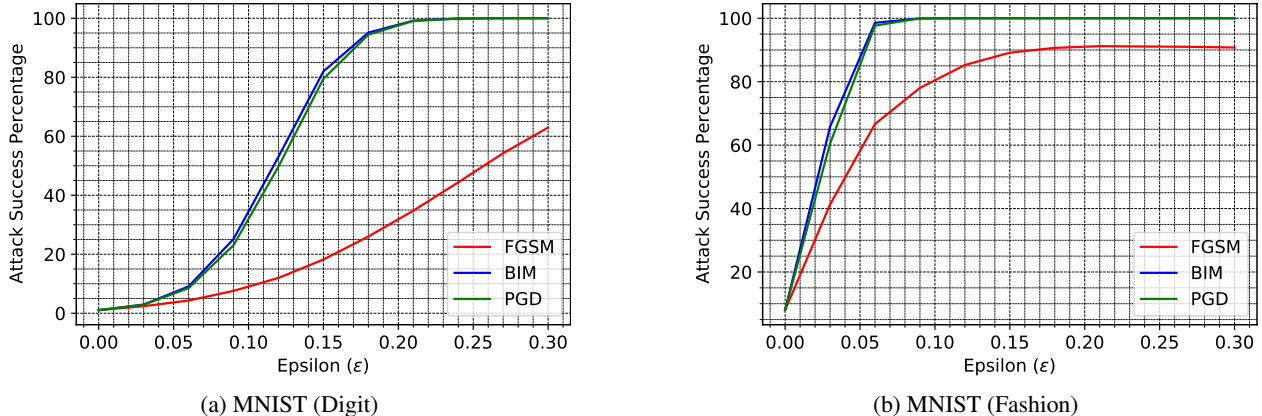


Figure 2: FGSM, BIM and PGD attacks success ratio.

As can be seen from the figure, BIM and PGD attacks converge to 100% and can successfully fool the model for all the input samples after an  $\epsilon$  value of about 0.2, whereas FGSM can only fool around 65% of all the images even it uses higher epsilon value.

## 3.3 Model Uncertainty in Bayesian Deep Learning

Given a dataset  $\mathcal{D} = \{(\mathbf{x}_1, y_1), \dots, (\mathbf{x}_N, y_N)\} \subset X \times Y$  where  $X \in \mathbb{R}^m$  is a  $m$ -dimensional input vector and  $Y \in \{1 \dots C\}$  where  $C$  is the output labels, training instances  $\{\mathbf{x}_i, y_i\} \forall X$  are a set of independent and identically distributed (i.i.d.) training samples from some unknown probability measure  $P$  on  $X \times Y$ . The objective is to find

a hypothesis  $h : X \mapsto Y$  using weights of neural net parameters  $w$  and a loss function  $\ell : Y \times Y \mapsto \mathbb{R}$  as close as possible to the original function that has generated the labels.

Gal et al. [24] showed that a neural network model with inference time dropout is equivalent to a specific variational inference on a Bayesian neural network model. The prediction hypothesis uncertainty is approximated by averaging probabilistic feed-forward Monte Carlo dropout sampling during the prediction time.

It acts as an ensemble approach. In each single ensemble model, the system has to drop out different neurons in the network's each layer according to the dropout ratio in the prediction time. The predictive mean is the average of the predictions over dropout iterations,  $T$ , and the predictive mean is used as the final inference,  $\hat{y}$ , for the input instance  $\hat{\mathbf{x}}$  in the dataset. The overall prediction uncertainty is approximated by finding the entropy and the variance of the probabilistic feed-forward Monte Carlo dropout sampling during prediction time. The prediction is defined as follows:

$$p(\hat{y} = c | \hat{\mathbf{x}}, \mathcal{D}) \approx \hat{\mu}_{pred} = \frac{1}{T} \sum_{y \in T} p(\hat{y} | \theta, \mathcal{D}) \quad (4)$$

where  $\theta$  is the model weights,  $\mathcal{D}$  is the input dataset,  $T$  is the number of predictions of the MC dropouts, and  $\mathbf{x}$  is the input sample. The label of input sample  $\mathbf{x}$  can be estimated with the mean value of Monte-Carlo dropouts predictions  $p(\hat{y} | \theta, \mathcal{D})$ , which will be done  $T$  times.

Figure 3 shows the general overview of the Monte Carlo dropout based classification algorithm in the prediction time. In the prediction time, random neurons in each layer are dropped out, according to the  $p$ , from the base neural network model to create another model. As a result,  $T$  different classification models can be used for the prediction of the input instance's class label and uncertainty quantification of the overall prediction.

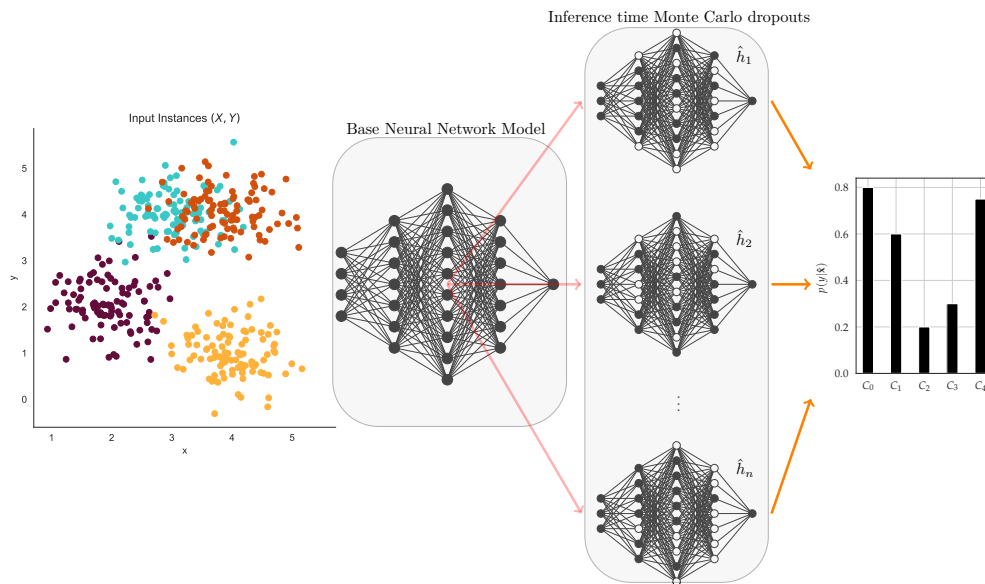


Figure 3: Illustration of the Monte Carlo dropout based Bayesian prediction.

For each testing input sample  $\mathbf{x}$ , the predicted label is assigned with the highest predictive mean.

### 3.4 Uncertainty metrics

In this study, we have used four different uncertainty metrics to quantify predictive uncertainty to detect adversarial samples: *confidence of the prediction*, *entropy*, *variance* and *mutual information*. We tried to understand the impact of these indicators and tested which one or the combination of these gives us the best performance.

### 3.4.1 Prediction Confidence

For an input image  $\mathbf{x}$ ,  $T$  different predictions is obtained  $p_t(\mathbf{x})$  by Monte-Carlo Dropout sampling where each prediction is a vector of softmax scores for the  $C$  classes. The next step is to compute the average prediction score for the  $T$  different outputs:

$$p_T(\mathbf{x}) = \frac{1}{T} \sum_{t \in T} p_t(\mathbf{x}) \quad (5)$$

And finally  $\max(p_T(x))$  gives us the confidence score for the predicted class.

### 3.4.2 Entropy

As a well-known concept from information technology, the entropy of a random variable is a measure of the average level of randomness or uncertainty inherent in the possible outcomes [25]. We compute entropy as below:

$$H(p_T(\mathbf{x})) = - \sum_{c \in C} p_T(\mathbf{x})[c] \log(p_T(\mathbf{x})[c]) \quad (6)$$

where  $p_T(\mathbf{x})$  is the average prediction score.

### 3.4.3 Variance

It is the expectation of the squared deviation of a random variable from its mean [26]. In our case, the first step is to compute the variance of the  $T$  predictions for each class.

$$\sigma^2(p_T(\mathbf{x})) = \frac{1}{T} \sum_{t \in T} (p_t(\mathbf{x}) - p_T(\mathbf{x}))^2 \quad (7)$$

Equation 7 gives us a vector where each element represents variance for related class. As the next step, we need to compute the expected value of variance over all classes by taking their average.

### 3.4.4 Mutual Information

Mutual information is computed as a difference between the entropy of the expected prediction, and the expectation of the model prediction entropy values across samples [27].

$$H(p_T(\mathbf{x})) - \frac{1}{T} \sum_{t \in T} \sum_{c \in C} (p_t(\mathbf{x})[c] \log(p_t(\mathbf{x})[c])) \quad (8)$$

### 3.4.5 Explanatory Research on Uncertainty Quantification Methods

We have made a simple test on a sample image to visualize how the uncertainty metrics obtained from MC Dropout estimate behave under an adversarial attack with varying strengths. Figure 4 shows how the uncertainty quantification values affected under an attack to our model with different allowed perturbation amounts,  $\epsilon$ .

We can see that variance, entropy and mutual information increases as the amount of perturbation applied to the image is high enough to fool the classifier. Likewise, the model's confidence gets lower for these  $\epsilon$  values. Indeed, the maximum variance, entropy, mutual info values and minimum confidence values are observed at an  $\epsilon$  value where the model starts mispredicting the input class. We call this interval as "low confidence interval". Moreover, when the amount of perturbation is limited, attack strength and success rate is low, or when the amount of perturbation used to fool the model is high, uncertainty values are not so reliable for detection. We call this interval as "high confidence interval". For those cases, we need additional indicators to help us to increase detection accuracy scores. To overcome the detection accuracy problem, we used two other different metrics as KL divergence loss and Kernel Density Estimation score for the last hidden layer activation's.

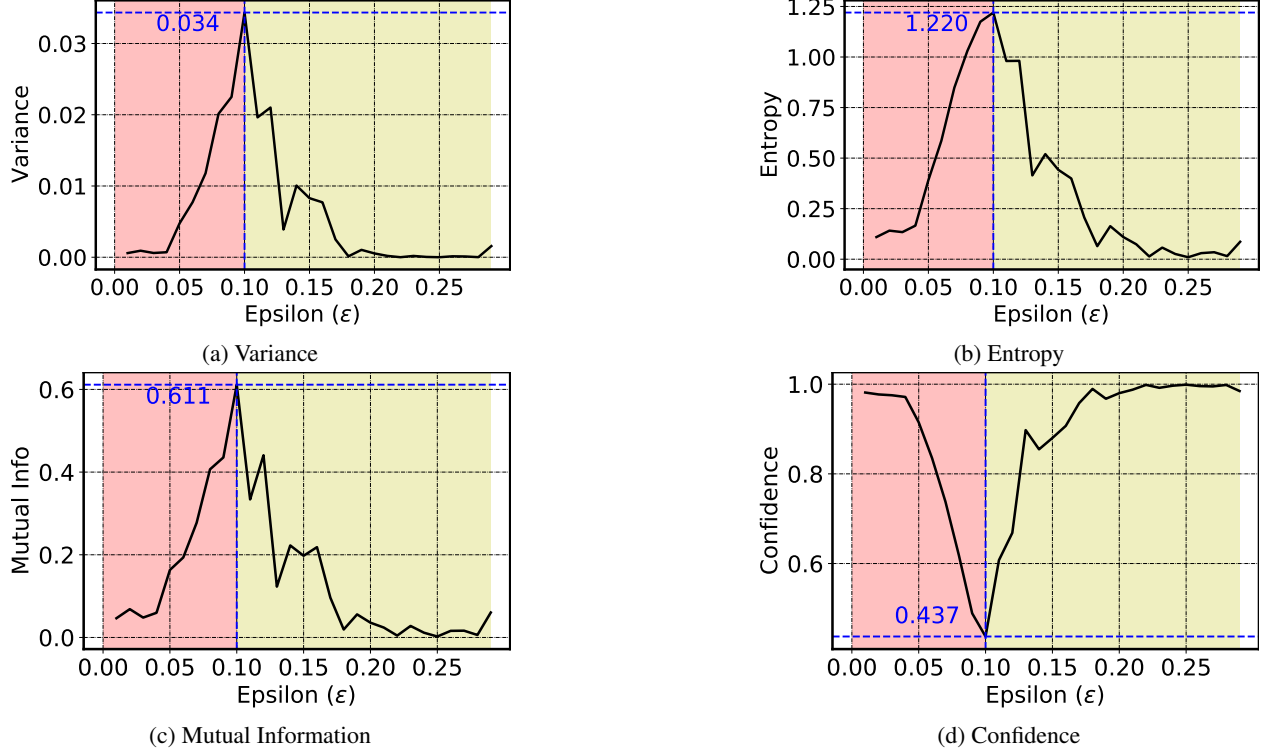


Figure 4: Change of uncertainty-based metrics under BIM attack with different amount of maximum allowed perturbation ( $\epsilon$ ) values.

### 3.5 Closeness metrics

Apart from the uncertainty metrics, one other possible way to understand the underlying mechanism of adversarial machine learning vulnerabilities, is to look at the manifold of the data used in the model training phase. Like all the other high dimensional data, input instances are also believed to lie on low dimensional data manifold. The adversarial attack pushes the input instance off from the source class' data manifold for the successful attack. The representation of the input instance in lower dimensional space (i.e. mapping from the high-dimensional input space to lower dimensional space) leave the data manifold of the source class and move towards the data manifold of the target class. Feinman et al. [15] suggested using Kernel Density Estimation (KDE) scores as an indicator of adversarial instance existence. They worked with the last hidden layer activations since this layer provides a space of acceptable dimensionality in which one can expect the manifold of the data to be simplified. In this study, we also used their approach and evaluated the usefulness of KDE method in different conditions. We have also introduced a new alternative approach based on KL Divergence Loss metric.

#### 3.5.1 Kernel Density Estimation

KDE is used as a measure to quantify how far an input sample is from the manifold that represents the distribution of that input class [28]. KDE can be described as:

$$\hat{K}(\mathbf{x}, X_c) = \sum_{\mathbf{x}_i \in X_c} k_\sigma(\phi(\mathbf{x}), \phi(\mathbf{x}_i)) \quad (9)$$

where  $\mathbf{x}$  is input instance,  $X_c$  is the training instances for class  $c$ ,  $k_\sigma$  is the kernel function (Gaussian kernel,  $\exp(-\|x - y\|^2 / \sigma^2)$ ),  $\phi(\mathbf{x})$  is the last hidden layer activation vector for instance  $\mathbf{x}$ ,

If the KDE value is high for the predicted class, that means the representation of input sample in the last hidden layer is close to the predicted class. Therefore, as the degree of adversarial perturbation and attack strength increases, the input instance is pushed to the decision boundary of the model, leaves the input class manifold and approaches to the target class manifold. Furthermore, we can track this journey through KD estimate of the input for source and predicted class as in Figure 5.

### 3.5.2 Kullback-Leibler Divergence

Kullback-Leibler Divergence (KL Divergence) is used to quantify how much one probability distribution differs from another probability distribution [29]. Let  $P$  and  $Q$  be two different probability distributions. In case of continuous distributions where  $P$  and  $Q$  are probability density function (PDF), KL divergence loss between  $P$  and  $Q$  can be shown as:

$$D_{KL}(P||Q) = \int P(\mathbf{x}) \log\left(\frac{P(\mathbf{x})}{Q(\mathbf{x})}\right) \quad (10)$$

In case of discrete distributions where  $P$  and  $Q$  are probability mass function (PMF), KL divergence loss between  $P$  and  $Q$  can be calculated as:

$$D_{KL}(P||Q) = \sum_i P(\mathbf{x}) \log\left(\frac{P(\mathbf{x})}{Q(\mathbf{x})}\right) \quad (11)$$

Like in the case of KDE, if we operate in the space of last hidden layer, we first find the expected value of PMF's for each class as:

$$Q_c = \frac{1}{N} \sum_{j \in N} q_j^c \quad (12)$$

where,  $N$  is the number of training samples for class  $c$ ,  $q_j^c$  is vector representation of last hidden layer activation of  $j$ th training instance of class  $c$ ,  $Q_c$  is mean (i.e. expected value) of last hidden layer activation outputs of all the training samples for class  $c$

The KL divergence based uncertainty quantification metric for the input instance  $\mathbf{x}$  is computed using the last hidden layer activation vector  $P_x$  and the mean vector  $Q_c$  of predicted class.

Note that both  $P$  and  $Q$  distributions are in PMF form and necessary conversions should be applied before computing KL Divergence Loss formula.

This metric can be regarded as the opposite of KDE. KDE measure gives how two distribution fit to each other, whereas KL Divergence Loss measure gives an idea about how two distributions differ from each other. So, high values of KL Divergence Loss for source or predicted class means that the input image is being pushed away from the corresponding data manifold.

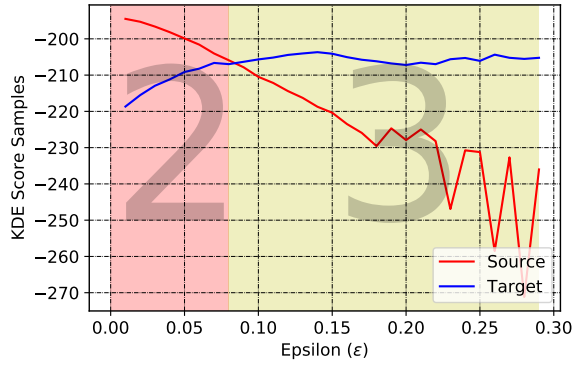
### 3.5.3 Explanatory Research on Closeness Metrics

Figure 5 shows the effectiveness of our proposed KDE based uncertainty quantification metrics. The x-axis shows the  $\epsilon$  values, and the y-axis shows the KDE values for BIM and FGSM attacks. In the upper left diagram, the crossing point for the blue line (target class) and the red line (source class) represents the  $\epsilon$  value of 0.09 where the misclassification has happened from class label 2 to label 3. As the amount of perturbation and attack strength increase, input sample representation in the last hidden layer starts to fit the distribution for target class rather than the source class. Thus, the KDE values for source and target class change in the opposite direction as expected.

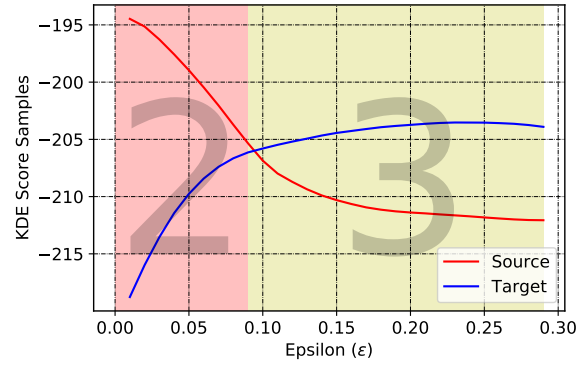
Figure 6 shows the KL Divergence Loss values of source and target classes to the input sample under BIM attack for different epsilon values. The crossing point for blue and red lines represents the epsilon value of 0.09, where the misclassification has started. As the amount of perturbation and attack strength increase, input sample representation in the last hidden layer starts to differ from the distribution for source and starts to resemble the distribution or target. Thus, the KL Divergence Loss estimates for source and target class change in the opposite direction as expected.

Figure 7 shows the KL Divergence Loss values of predicted class under BIM and FGSM attacks for different ( $\epsilon$ ) values. Since the strength of these attacks are different, and BIM is much stronger than FGSM, the final loss value for BIM attack at  $\epsilon = 0.30$  is quite lower than FGSM attack. That means, for BIM attack, the representation of adversarial sample at last hidden layer is much more close to the representation of predicted (target) class than in the case of FGSM. Moreover, this can be a sign that the model interprets the adversarial sample much more confidently as a wrong class for BIM.

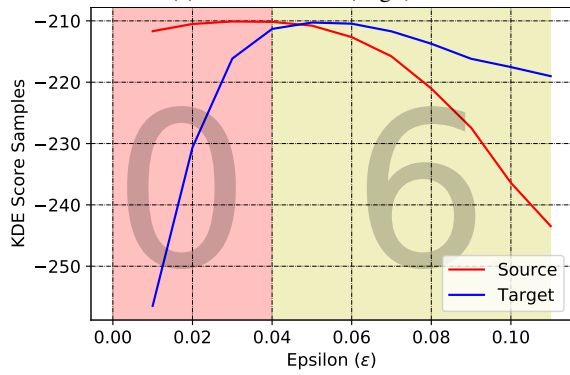




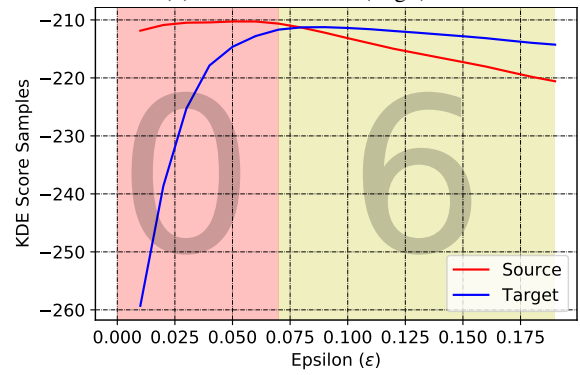
(a) BIM - MNIST (Digit)



(b) FGSM - MNIST (Digit)

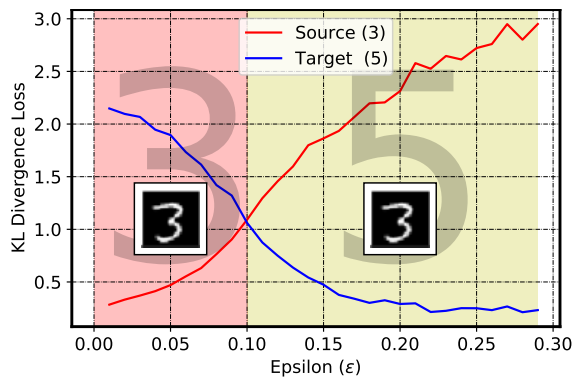


(c) BIM - MNIST (Fashion)

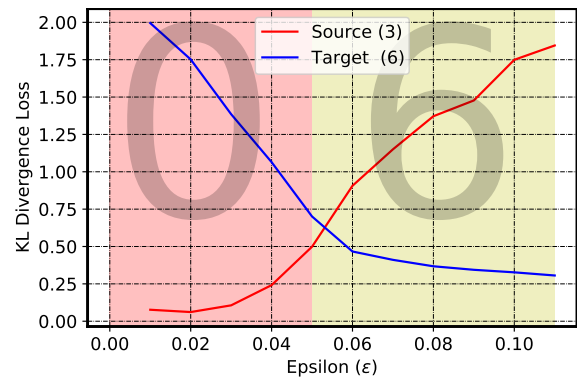


(d) FGSM - MNIST (Fashion)

Figure 5: KDE score changes of source and target classes with different  $\epsilon$  values.



(a) MNIST (Digit)



(b) MNIST (Fashion)

Figure 6: KL Divergence values of source and target classes under BIM attack with different amount of maximum allowed perturbation ( $\epsilon$ ) values. In the red section of the left figure, KL divergence loss of source class is lower than the target class' loss value. In this region the digit 3 is correctly predicted. In the red section where the target class' KL divergence loss value is higher than the source's value, the attack is successful, and the predicted class is 5.

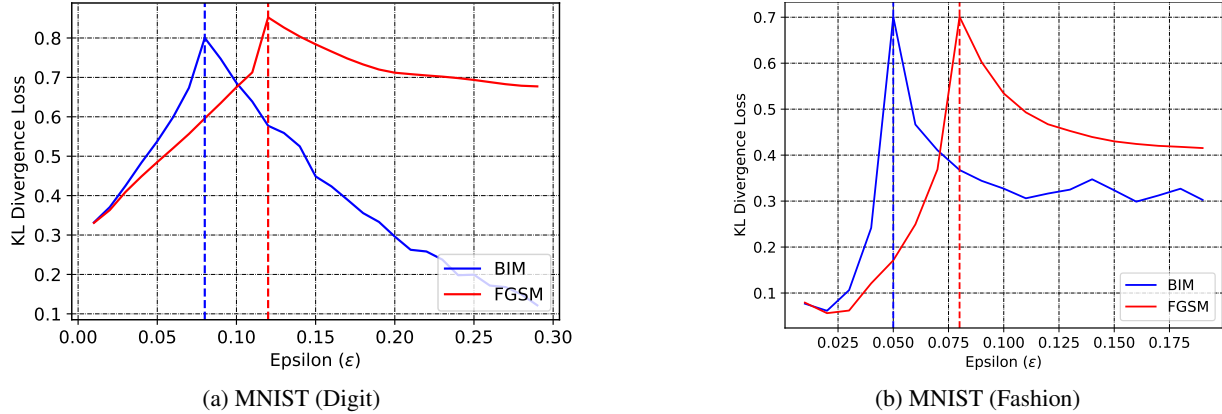


Figure 7: KL Divergence Loss values of *predicted* class under BIM and FGSM attack with different amount of maximum allowed perturbation ( $\epsilon$ ) values. The peaks of blue and red line graphs correctly show us the values of ( $\epsilon$ ) where a misclassification has actually happened for corresponding attack type.

## 4 System Model

### 4.1 Capability of The Attacker

We assumed that the primary purpose of the attacker is to evade the model by applying a carefully crafted perturbation to the input data. In a real-world scenario, this white-box setting is the most desired choice for an adversary that does not take the risks of being caught in a trap. The problem is that it requires the attacker to access the model from outside to generate adversarial examples. After manipulating the input data, the attacker can exploit the model’s vulnerabilities in the same manner as in an adversary’s sandbox environment. The classification model predicts the adversarial instances that are the attacker can convert some class labels as another class label (i.e. wrong prediction).

However, to prevent this manipulation from being easily noticed by the human eye, an optimization problem needs to be solved by the attacker to decide which regions in the input data must be changed. By solving this optimization problem using one of the available attack methods [12, 21, 23], the attacker aims to reduce the classification performance on the adversarial data as much as possible.

### 4.2 System Overview

An overview of the system model is depicted in Figure 8. We evaluated the performance of *uncertainty* and *closeness* metrics to detect adversarial examples. All the six different metrics from these two groups listed in Table 5 are obtained from the same model which we used in training and testing time. One of the notable advantages of our approach is that there is no need to train any other network to compute the features we use in adversarial detection. During test time, we obtain model prediction outputs as usual by using the model in evaluation mode (dropout is disabled). To compute MC dropout uncertainty metrics, we use the same model in training mode (dropout enabled with  $p = 0.5$ ) and get  $T = 50$  different prediction outputs. Furthermore, to compute closeness metrics, we used the same model but this time in evaluation mode (dropout disabled) again and calculated our model’s last hidden layer activations.

## 5 Experiments

### 5.1 Experimental Setup

We trained our CNN models for the MNIST (Digit) dataset [30] and MNIST (Fashion) dataset [31] and we achieved accuracy rates of 98.84% and 92.03% respectively. The model architectures are given in Table 1 and the hyperparameters selected in Table 2.

### 5.2 Uncertainty values without attack

We have used our trained classifier to predict all the samples of MNIST (Digit) test dataset. Out of 10,000 samples, only 116 of them were mispredicted. Then we have analyzed the values of various uncertainty metrics for all the correct and

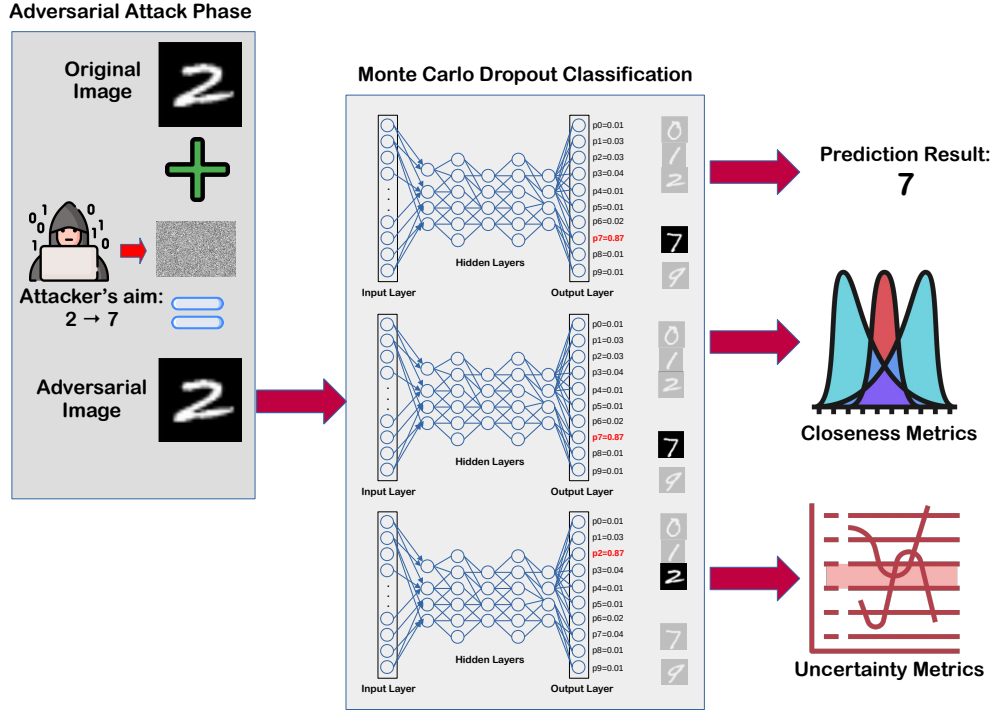


Figure 8: Overall System Model.

Table 1: CNN model architectures

Dataset	Layer Type	CNN Model
MNIST (Digit)	Convolution + ReLU	$3 \times 3 \times 10$
	Convolution + ReLU	$3 \times 3 \times 20$
	Max Pooling	$2 \times 2$
	Dropout	$p : 0.5$
	Fully Connected + ReLU	2880
	Dropout	$p : 0.5$
	Fully Connected + ReLU	128
	Output Layer	10
MNIST (Fashion)	Convolution (Padding = 1) + ReLU	$3 \times 3 \times 32$
	Max Pooling	$2 \times 2$
	Convolution (Padding = 0) + ReLU	$3 \times 3 \times 64$
	Max Pooling	$2 \times 2$
	Dropout	$p : 0.5$
	Fully Connected + ReLU	2304
	Dropout	$p : 0.5$
	Fully Connected + ReLU	600
	Fully Connected + ReLU	128
	Output Layer	10

wrong predictions. We observed that for the samples which were predicted correctly; variance, entropy and mutual info values are low, and model confidence is high. Furthermore, for the wrong predictions, uncertainty is high, and model confidence is low. The results are summarized in Table 3:

And when we used the same approach for MNIST (Fashion) dataset, we achieved the results listed in Table 4

Our results show that uncertainty indicators are indeed useful tools to evaluate the quality of the model predictions. Furthermore, using this fact, we can decide to let our models to abstain based on certain conditions like when our model's uncertainty is high, thus improving the reliability of the model.

Table 2: CNN model parameters used in both datasets

Parameter	CNN Model
Optimizer	Adam
Learning rate	0.001
Batch Size	64
Dropout Ratio	0.5
Epochs	10

Table 3: Uncertainty values of the model for the MNIST (digit) test data.

Expected value	Wrong Prediction	Correct Prediction
Variance	0.02195	0.00135
Entropy	0.96277	0.08891
Mutual Info	0.42247	0.04068
Confidence	0.59387	0.97724

Table 4: Uncertainty values of the model for the MNIST (fashion) test data.

Expected value	Wrong Prediction	Correct Prediction
Variance	0.00851	0.00189
Entropy	0.85190	0.021470
Mutual Info	0.15496	0.04173
Confidence	0.62365	0.92447

### 5.3 Adversarial Classification

To evaluate the performance of different metrics for adversarial detection, we have implemented each of the 3 attacks (FGSM, BIM, PGD) with different allowed perturbation amounts ( $\epsilon$ ) under  $l_{inf}$  norm on MNIST (Digit) and MNIST (Fashion) test data. To be consistent with Feinman et al. [15], we only perturbed those test samples which were correctly classified by our models in their original states. Because an adversary would have no reason to perturb samples that are already misclassified. For each adversarial sample, we have also included normal and noisy counterparts in the pool as a benchmark. We craft noisy samples by applying Gaussian noise to each pixel with a scale similar to the adversarial samples. Then, all these normal, noisy and perturbed samples are used to train a logistic regression model to test the performance of the adversarial classifier. Adversarial samples are labeled as 1, which represents the positive class, whereas normal and noisy samples are labeled as 0, which represents the negative class. Total of six features which are computed for each sample in the pool before LR training are shown in Table 5.

In order to capture model uncertainty for an input image  $x$ , we used dropout at prediction time with the probability of 0.5 and performed  $T = 50$  predictions where each prediction is a vector of softmax values for 10 different classes. Using these softmax scores, uncertainty metrics have been calculated for each clean, noisy and perturbed input samples. Moreover, to capture closeness metrics, we used the last hidden layer activation's of input samples while our model is in evaluation mode and computed Kernel Density Estimation (KDE) scores and KL Divergence Loss values for each sample. For KDE, we used a Gaussian kernel and a fixed bandwidth of 1.70 to fit our kernel density model to MNIST (Digit) training data, whereas in MNIST (Fashion) dataset, we used a bandwidth value of 1.00.

After computing all six different features for the whole dataset, we have tested them, using LR classifier and the effectiveness of each feature and possible combinations of them has been evaluated based on ROC-AUC measures. The results are shown in Figure 9 and 10

Table 5: All the features tested in LR Classifier for detecting Adversarial Samples

uncertainty-based metrics	closeness-based metrics
Variance	KDE
Entropy	KL Divergence
Mutual Info	
Confidence	

We know from Figure 2 that BIM or PGD attack with high  $\epsilon$  value like 0.30 results in %100 attack success rate and successfully fools the classifier for all the test inputs. When we analyzed the results shown in Figure 9, we can see

that for the cases where the attack is powerful, uncertainty metrics are not a useful tool to detect adversarial samples. Furthermore, the usage of closeness metrics, specifically KDE, performs much better. Because the uncertainty metrics lies in the “*high confidence interval*” and model prediction outputs are pushed far away from the decision boundary of the model, approaching to the target predicted class. Whereas, for BIM or PGD attack with low  $\epsilon$  values like 0.12 or for a weaker attack type like FGSM, the choice of uncertainty metrics over closeness metrics is much more effective. Moreover, within the uncertainty metrics, entropy and model confidence seem to perform slightly better than variance and mutual information. For the latter case where the attack strength is not very high, uncertainty metrics lie within the “*low confidence interval*”, and the model prediction outputs are not pushed far away from decision boundary of the model.

We also observed that the ensemble approach of using all the features combined instead of using only one of them increases AUC scores of LR classifier. Furthermore, although the complementary usage of KL Divergence Loss increases detection performance, it is not useful as Kernel Density Estimation(KDE). Because our KL Divergence Loss metric is a rough estimate of the actual distance between the two distributions in the space of last hidden unit activation’s, and it does not capture the true distance well enough to estimate the closeness criteria. Nevertheless, we also observe that KL Divergence Loss is useful than KDE for attacks with lower strengths.

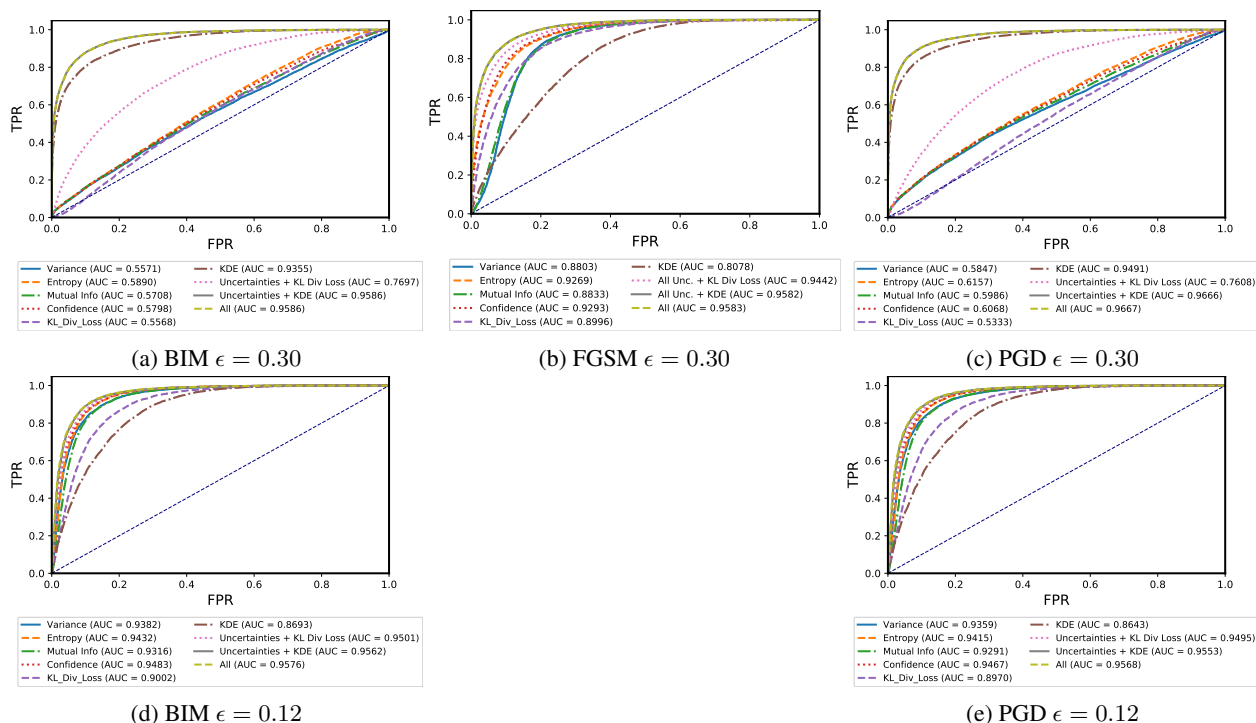


Figure 9: MNIST (Digit) ROC plots of FGSM, BIM and PGD attacks with 0.30 and 0.12  $\epsilon$  values.

## 6 Conclusion and Future Work

In this paper, we analyzed the usage of 6 different metrics for adversarial sample detection under 2 categories. We showed that the choice for the correct metric is significantly dependent on the degree of threat expected. We traced the better performers within each group and showed that the ensemble approach of combined usage of all metrics yield a better result in adversarial detection. Our results report that using all the metrics combined we can obtain a ROC-AUC score of up to %96.

In this work, we only focused on adversarial sample detection on independent, identically distributed (I.I.D.) data. However, in a real world scenario, as mentioned by Goodfellow [32] (2019), an adversary does not need to follow I.I.D assumption. Crafting only one adversarial sample and using this all the time can lower the accuracy rate of the prediction model down to zero in the long run. In future work, we plan to use the adversarial detection method to increase robustness for the aim of building a dynamic model that can be safely put in production.

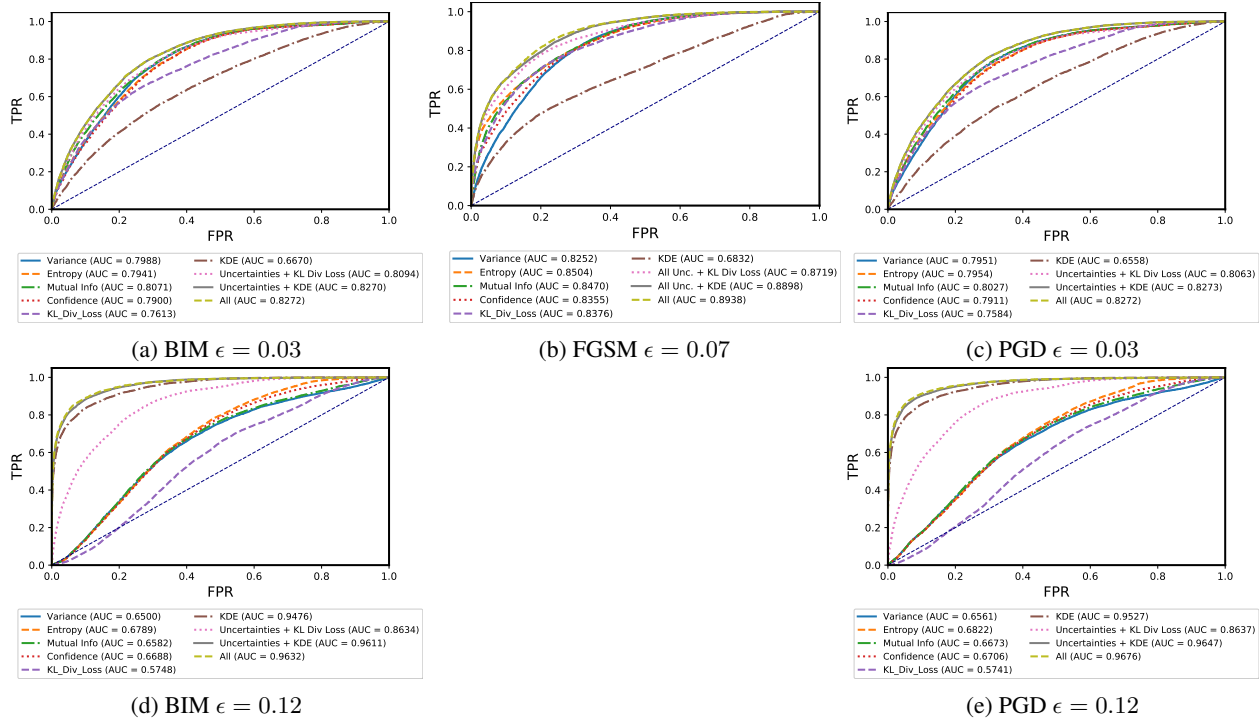


Figure 10: MNIST (Fashion) ROC plots of FGSM, BIM and PGD attacks with 0.03 and 0.12  $\epsilon$  values.

## References

- [1] Y. LeCun, Y. Bengio, G. Hinton, Deep learning, *Nature* 521 (7553) (2015) 436–444.
- [2] W. T. Le, F. Maleki, F. P. Romero, R. Forghani, S. Kadoury, Overview of machine learning: Part 2: Deep learning for medical image analysis, *Neuroimaging Clinics of North America* 30 (4) (2020) 417 – 431, machine Learning and Other Artificial Intelligence Applications. doi:<https://doi.org/10.1016/j.nic.2020.06.003>.
- [3] V. Sharma, R. N. Mir, A comprehensive and systematic look up into deep learning based object detection techniques: A review, *Computer Science Review* 38 (2020) 100301. doi:<https://doi.org/10.1016/j.cosrev.2020.100301>.
- [4] M. B. Akçay, K. Oğuz, Speech emotion recognition: Emotional models, databases, features, preprocessing methods, supporting modalities, and classifiers, *Speech Communication* 116 (2020) 56 – 76.
- [5] H. Li, G. Li, Y. Yu, Rosa: Robust salient object detection against adversarial attacks, *IEEE Transactions on Cybernetics* 50 (11) (2020) 4835–4847. doi:[10.1109/TCYB.2019.2914099](https://doi.org/10.1109/TCYB.2019.2914099).
- [6] Y. Wang, Y. an Tan, W. Zhang, Y. Zhao, X. Kuang, An adversarial attack on dnn-based black-box object detectors, *Journal of Network and Computer Applications* 161 (2020) 102634. doi:<https://doi.org/10.1016/j.jnca.2020.102634>.
- [7] S. G. Finlayson, H. W. Chung, I. S. Kohane, A. L. Beam, Adversarial attacks against medical deep learning systems (2019). arXiv:1804.05296.
- [8] C. Sitawarin, A. N. Bhagoji, A. Mosenia, M. Chiang, P. Mittal, Darts: Deceiving autonomous cars with toxic signs (2018). arXiv:1802.06430.
- [9] N. Morgulis, A. Kreines, S. Mendelowitz, Y. Weisglass, Fooling a real car with adversarial traffic signs (2019). arXiv:1907.00374.
- [10] C. Szegedy, W. Zaremba, I. Sutskever, J. Bruna, D. Erhan, I. Goodfellow, R. Fergus, Intriguing properties of neural networks (2014). arXiv:1312.6199.
- [11] X. Huang, D. Kroening, W. Ruan, J. Sharp, Y. Sun, E. Thamo, M. Wu, X. Yi, A survey of safety and trustworthiness of deep neural networks: Verification, testing, adversarial attack and defence, and interpretability, *Computer Science Review* 37 (2020) 100270. doi:<https://doi.org/10.1016/j.cosrev.2020.100270>.

- [12] I. J. Goodfellow, J. Shlens, C. Szegedy, Explaining and harnessing adversarial examples (2015). arXiv:1412.6572.
- [13] N. Papernot, P. McDaniel, X. Wu, S. Jha, A. Swami, Distillation as a defense to adversarial perturbations against deep neural networks (2016). arXiv:1511.04508.
- [14] N. Carlini, D. Wagner, Towards evaluating the robustness of neural networks (2017). arXiv:1608.04644.
- [15] R. Feinman, R. R. Curtin, S. Shintre, A. B. Gardner, Detecting adversarial samples from artifacts (2017). arXiv:1703.00410.
- [16] X. Ma, B. Li, Y. Wang, S. M. Erfani, S. Wijewickrema, G. Schoenebeck, D. Song, M. E. Houle, J. Bailey, Characterizing adversarial subspaces using local intrinsic dimensionality (2018). arXiv:1801.02613.
- [17] J. H. Metzen, T. Genewein, V. Fischer, B. Bischoff, On detecting adversarial perturbations (2017). arXiv:1702.04267.
- [18] M. Combalia, F. Hueto, S. Puig, J. Malvehy, V. Vilaplana, Uncertainty estimation in deep neural networks for dermoscopic image classification, in: 2020 IEEE/CVF Conference on Computer Vision and Pattern Recognition Workshops (CVPRW), 2020, pp. 3211–3220. doi:10.1109/CVPRW50498.2020.00380.
- [19] C. Leibig, V. Allken, M. S. Ayhan, P. Berens, S. Wahl, Leveraging uncertainty information from deep neural networks for disease detection, bioRxiv (2017). arXiv:https://www.biorxiv.org/content/early/2017/10/18/084210.full.pdf.
- [20] N. Akhtar, A. Mian, Threat of adversarial attacks on deep learning in computer vision: A survey, IEEE Access 6 (2018) 14410–14430. doi:10.1109/ACCESS.2018.2807385.
- [21] A. Kurakin, I. Goodfellow, S. Bengio, Adversarial examples in the physical world (2017). arXiv:1607.02533.
- [22] A. Kurakin, I. J. Goodfellow, S. Bengio, Adversarial machine learning at scale, CoRR abs/1611.01236 (2016). arXiv:1611.01236.
- [23] A. Madry, A. Makelov, L. Schmidt, D. Tsipras, A. Vladu, Towards deep learning models resistant to adversarial attacks (2019). arXiv:1706.06083.
- [24] Y. Gal, Z. Ghahramani, Dropout as a bayesian approximation: Representing model uncertainty in deep learning (2016). arXiv:1506.02142.
- [25] C. E. Shannon, A mathematical theory of communication, The Bell System Technical Journal 27 (1948) 379–423, 623–656.
- [26] M. Loeve, Probability theory i, volume 45 of, Graduate texts in mathematics 4 (1977).
- [27] T. Nair, D. Precup, D. L. Arnold, T. Arbel, Exploring uncertainty measures in deep networks for multiple sclerosis lesion detection and segmentation (2018). arXiv:1808.01200.
- [28] Y. He, Y. Mao, W. Chen, Y. Chen, Nonlinear metric learning with kernel density estimation, IEEE Transactions on Knowledge and Data Engineering 27 (6) (2015) 1602–1614.
- [29] D. J. MacKay, D. J. Mac Kay, Information theory, inference and learning algorithms, Cambridge university press, 2003.
- [30] Y. LeCun, C. Cortes, MNIST handwritten digit database (2010). URL <http://yann.lecun.com/exdb/mnist/>
- [31] H. Xiao, K. Rasul, R. Vollgraf, Fashion-mnist: a novel image dataset for benchmarking machine learning algorithms (2017). arXiv:1708.07747.
- [32] I. Goodfellow, A research agenda: Dynamic models to defend against correlated attacks (2019). arXiv:1903.06293.